IEEE Access
Multidisciplinary ⋮ Rapid Review ⋮ Open Access Journal

Received May 25, 2020, accepted June 3, 2020, date of publication June 8, 2020, date of current version June 25, 2020.

Digital Object Identifier 10.1109/ACCESS.2020.3000481

From Coarse to Fine (FC2F): A New Scheme of Colorizing Thermal Infrared Images

FEIYAN CHENG[1,2,3], JUNSHENG SHI[1,3], (Member, IEEE), LIJUN YUN[2], XUEBING CAO[1], AND JUN ZHANG[1,3]

[1]School of Physics and Electronic Information, Yunnan Normal University, Kunming 650500, China
[2]School of Information Science and Technology, Yunnan Normal University, Kunming 650092, China
[3]Yunnan Key Laboratory of Optoelectronic Information Technology, Kunming 650500, China

Corresponding authors: Junsheng Shi (shijs@ynnu.edu.cn) and Jun Zhang (junzhang@ynnu.edu.cn)

This work was supported in part by the National Natural Science Foundation of China under Grant 61875171, and in part by the Yunnan Key Lab of Opto-Electronics Information Technology, Kunming, China.

ABSTRACT Colorization of the thermal infrared image is an unsolved problem because usually there is no one-to-one relationship between an object's color and its temperature. In this paper, we propose a new colorization scheme to address this problem. We first create a coarse colorization image that maintains cross-correlation between its RGB channels. Then the matrix of shift, rotation, and scaling between the coarse colorization image and a source natural color image is constructed. Finally, the transformations act on the coarse colorization image to obtain the resultant image, which has the appearance of the source image. Experiments demonstrate the effectiveness of the new scheme and show its superiority to other state-of-the-art methods. The new scheme can be easily extended to the colorization of low illumination images and near-infrared images.

INDEX TERMS Infrared image, color night vision, colorization.

I. INTRODUCTION

Camera and video surveillance systems should work perfectly even in poor lighting and weather conditions. However, poor capture quality under these special conditions often prevents the system from being used for critical applications. The infrared imaging system can overcome some of the natural limits of light and weather conditions. Working properly under these special conditions can deeply benefit from the exploitation of such data. And infrared imaging systems have become more popular than ever before due to their lower prices. It has been more and more closely related with people's daily lives and widely used in all fields of life [1]–[3]. Figure 1 provides an example. It can be seen that many details have been almost buried in the dark and color information has been completely lost in an infrared image. There are two challenges for the infrared imaging system. One is that the imaging quality is usually poor, which generally has a low signal-to-noise ratio, low contrast, blurred edges and poor detail. It is important to enhance infrared images, and the enhanced images could be more useful for computer analysis and processing. The other is that infrared images are monochromatic and are usually presented as a grayscale image. Thousands of colors can be distinguished by the human visual system, while only about 100 levels of grayscale can be perceived. This is a serious drawback in real-world applications.

FIGURE 1. An infrared image (Left) is colorized (Right) by the new scheme presented in this paper. Better perception in color and details.

To make the buried information and color discrimination visible again, the enhancement and colorization technology is demanded. It shares some ideas with those approaches developed for grayscale image colorization or color transfer functions. In recent years, several approaches of image colorization have been proposed [4]–[11]. The existing techniques can be categorised according to the ways of obtaining and treating the data for modelling the correspondences between

The associate editor coordinating the review of this manuscript and approving it for publication was Shiping Wen.

an input image and a color image. Reinhard *et al.* [12] proposed a global approach that allowed you to obtain sunset images without waiting for dusk. This technique matches the mean and variance between the two images. Inspired by Reinhard *et al.*, Xiao and Ma [13] treated the RGB value of a pixel as a three-dimensional random variable. The mean and covariance matrix are calculated along three axes of RGB. They demonstrate that the parameters of the target image's colorization can be obtained by the covariance between the three components. Inspired by Xiao *et al.*'s work, we can infer that the correlations between the three components of the RGB space imply the color appearance characteristics of the image.

The biggest challenge of the infrared image's colorization is that there is no corresponding relationship between an object's color and its temperature. This inherent distinction is a major challenge when one goes to colorize an infrared image. Hence, it is necessary to turn to other features that imply the color appearance rather than its grayscale. The correlation between the three components of the RGB space is a new perfect breakthrough to extract and gather overall color information. In this paper, we try to generate clear details and natural RGB representation like daytime images. The methodology considers the infrared image as an R channel in RGB space. Then apply the correlations between the three components to construct B channel and G channel. This process is called coarse colorization, turning a single-channel infrared image into a color image. Transforming the infrared image into correlation space make it more clear and give us the better ability of colorization. Finally, an algorithm which is originally applied for color transfer between color images can be perfectly applied. Furthermore, our method can be easily extended to the colorization for low illumination images and near-infrared images.

In summary, this paper makes the following contributions:

- A new colorization scheme is proposed to improve the quality of thermal infrared images. The new scheme innovatively fuse the information of cross-correlation spaces and statistical characteristics.
- The new scheme is explainable about the physical similarity between an inverted infrared image and a haze image. We offer a reliable physical explanation from the principle of physical imaging.
- A set of well designed experiments are conducted to confirm the effectiveness of the new scheme. The new scheme has wide applications such as the near-infrared image colorization and the low illumination image colorization.

The remaining of the paper is organized as follows. Section 2 reviews the related work; In section 3, the proposed scheme is presented in details; Then, a reasonable physical explanation for the similarity between a haze image and an inverted infrared image is provided in section 4. Experimental results and analysis are reported in section 5. Finally, section 6 concludes the work.

II. RELATED WORK

A. TRADITIONAL METHODS

Colorization technique has been largely studied in recent years. It has been studied for transferring color to another color image, grayscale image, near-infrared image and thermal infrared image. Reinhard *et al.* [12] proposed a global approach that allowed you to obtain sunset images without waiting for dusk. This technique matches the mean and variance between the two images. Each pixel in the corresponding images participates in the calculation of the above two statistical variables, so it is called a global algorithm. Inspired by Reinhard *et al.*, Welsh *et al.* [14] employs neighbourhood matching criteria to realize the transmission of similar colour information from the reference image to the target image. Furthermore, Li *et al.* [15] proposes an algorithm to improve the matching accuracy by enhancing luminance contrast, which can improve the quality of the night image. The histogram matching algorithm is also thriving. A series of 1D histograms or a statistic for each histogram bin makes some matches [16], [17]. These methods share the limitation that the colorization quality relies heavily on the correspondence between color distribution and grayscale distribution.

B. DEEP NETWORK-BASED METHODS

Recently, convolutional neural networks (CNN) have become dominant methods in almost all computer vision tasks [18]–[22]. Therefore, we can find some new deep learning-based image colourization method. For example, we can refer to the process described in [23]. It renders natural images using a convolutional neural network (CNN). They annotated the SUN dataset [24], generated Scene Labels as additional features, and performed class-specific coloring better with the extracted DAISY features [25]. This approach is fully automated but requires Scene Labels. However, usually the input image we provide arbitrarily is missing Scene Labels, which is a limitation of the algorithm. Iizuka *et al.* [26] proposed a technique combining global prior knowledge and local image features. The local information contained in the small image blocks and the global prior details dependent on the entire image are merged by the fusion layer. This end-to-end architecture can process images without resolution requirements. The existing database with large scene classification is employed as the training dataset, and the classification label of the dataset is exploited to learn global priors more discriminatively. Sun *et al.* [27] proposed a technology to realize the cross-domain conversion from NIR to RGB through asymmetric periodic generation countermeasures network (ACGAN). In this work, they solved the problem of converting NIR to RGB fields and producing reasonable RGB images from NIR images. RGB images have more information than NIR images. All in all, One of the disadvantages of deep learning is that the algorithm requires a large account of data sets as training samples, but it is very difficult to make a training sample set that meets the actual needs. The other of the disadvantages is that the

subtle changes of network parameters during training will affect the performance of the whole network. Therefore, finding the best network is very time-consuming. In order to reduce the number of parameters and improve the performance, a group lasso and an in group lasso were developed to achieve sparse representation [28].

In this paper, we propose a novel, simple and effective enhancement and colorization scheme for infrared images. Firstly, a coarse colorization method is proposed. Then Xiao's method [13] is adopted to realize the transmission of color features across images. This method is robust to illumination because it requires the image statistical characteristics to calculate the scale, rotate and shift parameter rather than the pixel's illumination. The experimental results prove the effectiveness of our method. Our algorithm can be easily extended to the low illumination image colorization and the near infrared image colorization.

III. NEW COLORIZATION SCHEME

This section presents a new colorization scheme (FC2F), which has two stages-coarse colorization and fine colorization. Correlation information has shined in many fields [29]–[31], and we also used correlation information to build new solutions.

One significant characteristic of the natural image is high correlation between its components: about 0.78 for ρ_{rb}(cross-correlation between the R and B channel),0.98 for ρ_{rg} and 0.94 for ρ_{gb} [32]. ρ_{rb}, ρ_{rg} and ρ_{gb} can be calculated by (1):

$$\rho_{xy} = \frac{\sum_{i=1}^{n}(x_i-\bar{x})(y_i-\bar{y})}{\sqrt{\sum_{i=1}^{n}(x_i-\bar{x})^2}\sqrt{\sum_{i=1}^{n}(y_i-\bar{y})^2}}, \tag{1}$$

where n is the total sample number of an image; x_i and y_i are the individual sample points indexed with i taken either from R, G, or B channel; $\bar{x} = \frac{1}{n}\sum_{i=1}^{n} x_i$ is the sample mean; and analogously for $\bar{y}$.

Consequently, we prefer to build a coarse colorization image which has a strong correlation between R_{coarse}, G_{coarse} and B_{coarse}, as shown in Figure 2 (a). This process is called **coarse colorization**. The correlation coefficients between the three components of the coarse colorization image are shown in Figure 3. The correlation is measured by covariance. The covariance matrix is hired to find the transformation parameter between the coarse colorization image and the reference image with natural color presentation, as shown in Figure 2 (b). This process is called **fine colorization**.

A. COARSE COLORIZATION METHOD

The following model creates an coarse colorization image:

$$\begin{bmatrix} R_{coarse} \\ G_{coarse} \\ B_{coarse} \end{bmatrix} = \begin{bmatrix} T_r\{I\} \\ T_g\{I\} \\ T_b\{I\} \end{bmatrix}, \tag{2}$$

where I is an infrared image; T_r, T_g, T_b represents the transformation for R, G, B channel, respectively; R_{coarse}, G_{coarse} and B_{coarse} are the three components of the desired coarse colorization image.

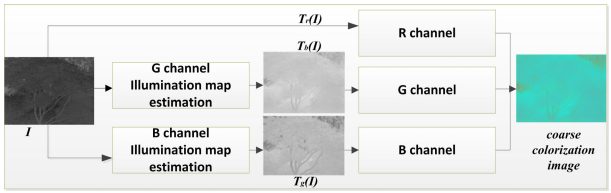

(a) Coarse colorization pipeline

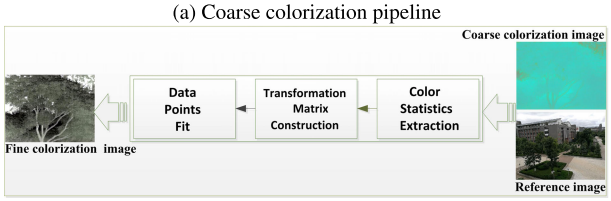

(b) Fine colorization pipeline

FIGURE 2. The flowchart of the proposed scheme.

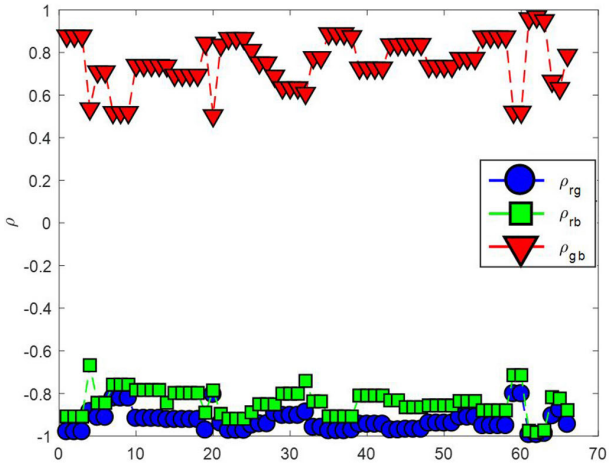

FIGURE 3. The correlation coefficients between the three components of the coarse colorization image.

1) R CHANNEL ILLUMINATION MAP ESTIMATION

We adapt the original image as the R channel:

$$T_r(I) \leftarrow I, \tag{3}$$

where I is an infrared image.

We post the original image into the R channel and perform different processing on the original image to generate the other two channels. Each component of the coarse colorization image should not only carry the luminance information but also be related to each other. All three channels are derived from the original image to guarantee the relationship.

2) B CHANNEL ILLUMINATION MAP ESTIMATION

In this paper, to deal with non-uniform lighting, the following estimation is adopted:

$$T_b(I) \leftarrow 255 - \max_{y\in\Omega(x)}\left(I\left(y\right)\right), \tag{4}$$

where I is an infrared image and $\Omega(x)$ is a local patch centered at x; The operator $\max_{y\in\Omega(x)}$ is a maximum filter.

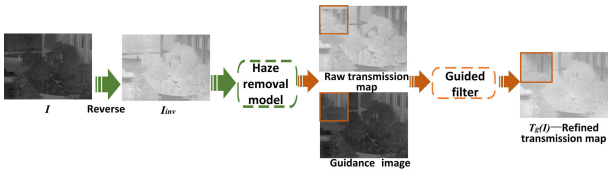

FIGURE 4. The scheme for G channel.

The inverse operation is to swap the target and the background in the infrared image. Then the B channel is complementary to the R channel. The background area in the infrared image is mostly black pixels. The R channel cannot reflect this information.

In this work, considering its simplicity, we hire (4) to estimate B channel illumination map. The maximum filtering strategy can enhance local consistency to some extent, but it is structurally blind. In the following sections, there will be a more powerful strategy to remedy this limitation.

3) G CHANNEL ILLUMINATION MAP ESTIMATION

It is a challenge to retain the overall structure while still having texture details. To achieve this goal, we develop a new scheme for the G channel. As mentioned in [33]–[35], the inverted infrared image and the low illumination image look similar to the haze image.

The inverted infrared image can be substituted into the haze imaging model to estimate the transmission map for dehazing. The guided filter is applied to enhance the transmission map. We call it 'Refined Transmission Map' and take it as the G channel. It has a strong correlation with the other two channels. Furthermore, the image details are enhanced. The description of the G channel scheme is described in Figure 4. For the input infrared image $I_{infrared}\,(x, y)$, we invert it using:

$$I_{inv}\,(x, y) = 1 - I_{infrared}\,(x, y)\,, \tag{5}$$

where $I_{inv}\,(x, y)$ is the intensity of the inverted infrared image. $I_{infrared}\,(x, y)$ is the intensity of the input infrared image at pixel (x, y).

The transmission map can be estimated [36] on $1 - I_{\text{inf}\,rared}$ as follow:

$$t\,(x, y) = 1 - w \min_{y \in \Omega(x)} \left(\frac{I_{inv}\,(y)}{A} \right), \tag{6}$$

The transmission map obtained from (6) is a raw transmission map which may contain some halo effects. Guided filter is the most widely used method to solve this problem [37]–[39]. In [40], a simple method was applied to filter the raw transmission map under the guidance of the hazy image. However, the texture details of the hazy image itself are blurred, which will cause incomplete haze removal. The choice of guided images is very important. The transmission map mainly depends on the **scene depth**. **Infrared images can be treated as a reference for the scene depth because heat decays with distance**. The unique features of infrared images are low contrast and low resolution, which make the infrared image contain more homogenous regions, with good spatial correlation. It captures the requirements of the uniform attribute in a local patch for the ideal transmission map. We prefer the infrared image itself as the guide image for refining a raw transmission map.

As mentioned in [40], the filtering output is expressed as a weighted average:

$$T_g(I) \leftarrow \sum_{(m,n) \in W_{ij}} W_{mn}(I_{infrared}) t_{mn}, \tag{7}$$

where i and j are pixel indexes. The filter kernel $W_{mn}(I_{infrared})$ is a function of the guidance image $I_{infrared}$ and independent of t. This filter is linear with respect to t. $I_{infrared}$ is the guidance image. t is the original image which represents the coarse transmission map $t(x, y)$. $T_g(I)$ is the output image which represents the refined transmission map. The refined transmission map is treated as the G channel illumination map estimation, as shown in Figure 4. The detail is enhanced while some halo effects are eliminated.

B. FINE COLORIZATION METHOD

In this paper, we apply Xiao *et al.*'s method [13] to conduct fine colorization. The RGB value of a pixel is statistically treated as a three-dimensional random variable. The mean and covariance matrix are calculated along three axes of RGB. The data points can be scaled, rotated and shifted to make the target image data cluster fitting into the RGB color space of the source image. The target image refers to the coarse colorization image. The source image refers to the reference image with natural color presentation.

The algorithm steps are as follows:

1) First, the mean and covariance for both the source and target images are calculated and denoted by $(\overline{R_{src}}, \overline{G_{src}}, \overline{B_{src}})$, $(\overline{R_{tgt}}, \overline{G_{tgt}}, \overline{B_{tgt}})$, Cov_{src} and Cov_{tgt} respectively.
2) Then, the covariance matrices are decomposed using the SVD algorithm. U_{src}, U_{tgt}, Λ_{src} and Λ_{tgt} are obtained.

$$Cov = U \cdot \Lambda \cdot V^T = \sum_{i=1}^{r} \sqrt{\lambda_i} u_i v_i, \tag{8}$$

3) Last, a transformation is defined as follow:

$$I = T_{src} \cdot R_{src} \cdot S_{src} \cdot S_{tgt} \cdot R_{tgt} \cdot T_{tgt} \cdot I_{tgt}, \tag{9}$$

where $I = (R, G, B, 1)^T$ and $I_{tgt} = (R_{tgt}, G_{tgt}, , B_{tgt}, 1)^T$ denote the result and target images matrices, respectively; T_{src},T_{tgt},R_{src},R_{tgt},S_{src} and S_{tgt} represent translation, rotation and scaling parameters. Here are their definitions:

$$T_{src} = \begin{pmatrix} 1 & 0 & 0 & t_{src}^r \\ 0 & 1 & 0 & t_{src}^g \\ 0 & 0 & 1 & t_{src}^b \\ 0 & 0 & 0 & 1 \end{pmatrix}, \tag{10}$$

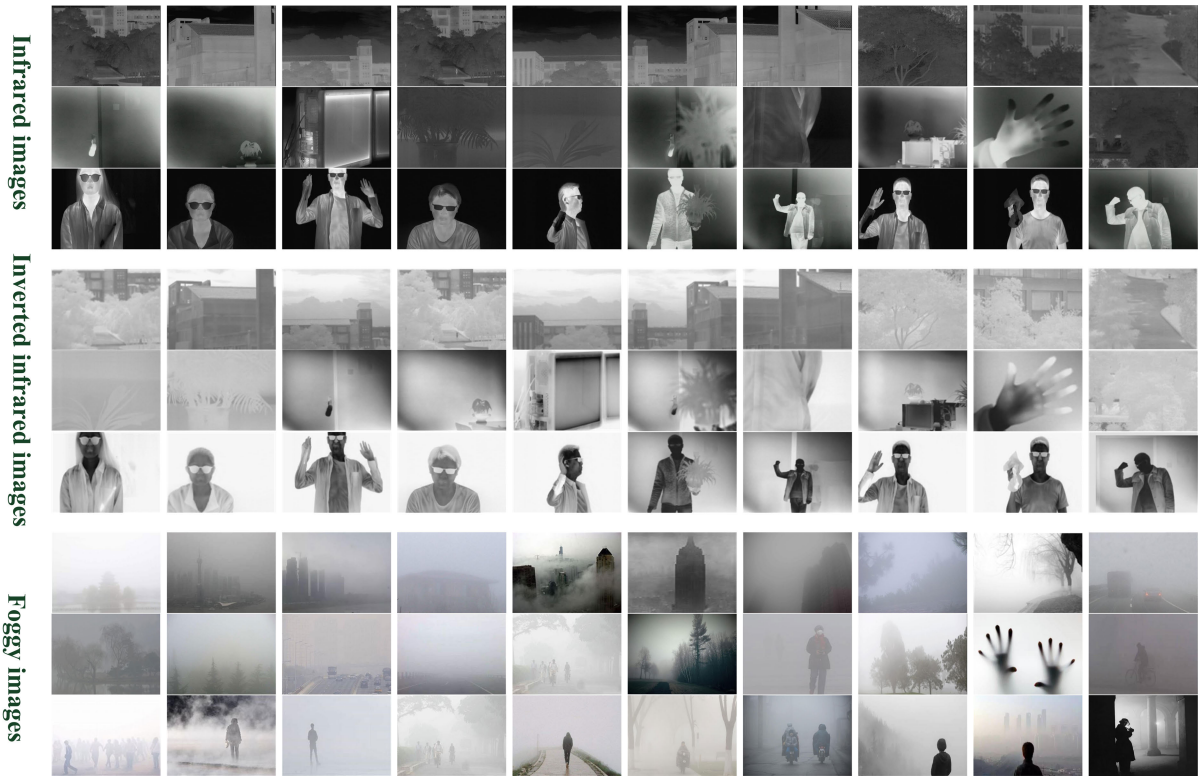

FIGURE 5. Infrared images, inverted infrared images and foggy images with a similar scene or style.

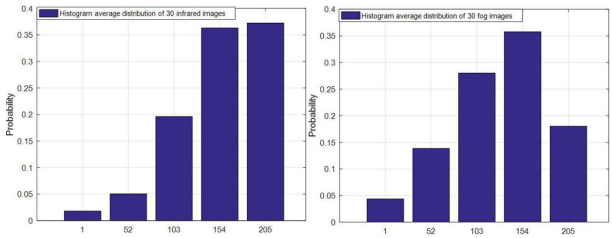

FIGURE 6. The comparison of the intensity histogram.

$$T_{tgt} = \begin{pmatrix} 1 & 0 & 0 & t^r_{tgt} \\ 0 & 1 & 0 & t^g_{tgt} \\ 0 & 0 & 1 & t^b_{tgt} \\ 0 & 0 & 0 & 1 \end{pmatrix}, \tag{11}$$

$$R_{src} = U_{src}, \tag{12}$$

$$R_{tgt} = U^{-1}{}_{tgt}, \tag{13}$$

$$S_{src} = \begin{pmatrix} s^r_{src} & 0 & 0 & 0 \\ 0 & s^g_{src} & 0 & 0 \\ 0 & 0 & s^b_{src} & 0 \\ 0 & 0 & 0 & 1 \end{pmatrix}, \tag{14}$$

$$S_{tgt} = \begin{pmatrix} s^r_{tgt} & 0 & 0 & 0 \\ 0 & s^g_{tgt} & 0 & 0 \\ 0 & 0 & s^b_{tgt} & 0 \\ 0 & 0 & 0 & 1 \end{pmatrix}, \tag{15}$$

where $t^r_{src} = \overline{R_{src}}$, $t^g_{src} = \overline{G_{src}}$, $t^b_{src} = \overline{B_{src}}$, $t^r_{tgt} = -\overline{R_{tgt}}$, $t^g_{tgt} = -\overline{G_{tgt}}$, $t^b_{tgt} = -\overline{B_{tgt}}$, $S^r_{src} = \lambda^R_{src}$, $s^g_{src} = \lambda^G_{src}$, $s^b_{src} = \lambda^B_{src}$, $s^r_{tgt} = 1\Big/\sqrt{\lambda^R_{tgt}}$, $s^g_{tgt} = 1\Big/\sqrt{\lambda^G_{tgt}}$ and $s^b_{tgt} = 1\Big/\sqrt{\lambda^B_{tgt}}$.The subscripts of *src* and *tgt* represent for source image and target image, respectively.

FIGURE 7. Hardware platform.

The fine colorization acts on all of the pixels in the coarse colorization image and moves them to fit the source image. Then, the color distribution of the fine colorization image becomes more abundant.

IV. EXPLAINABLE THEORETICAL STUDY

Even though the some methods can produce excellent results, the basic model they rely on is lacking in physical

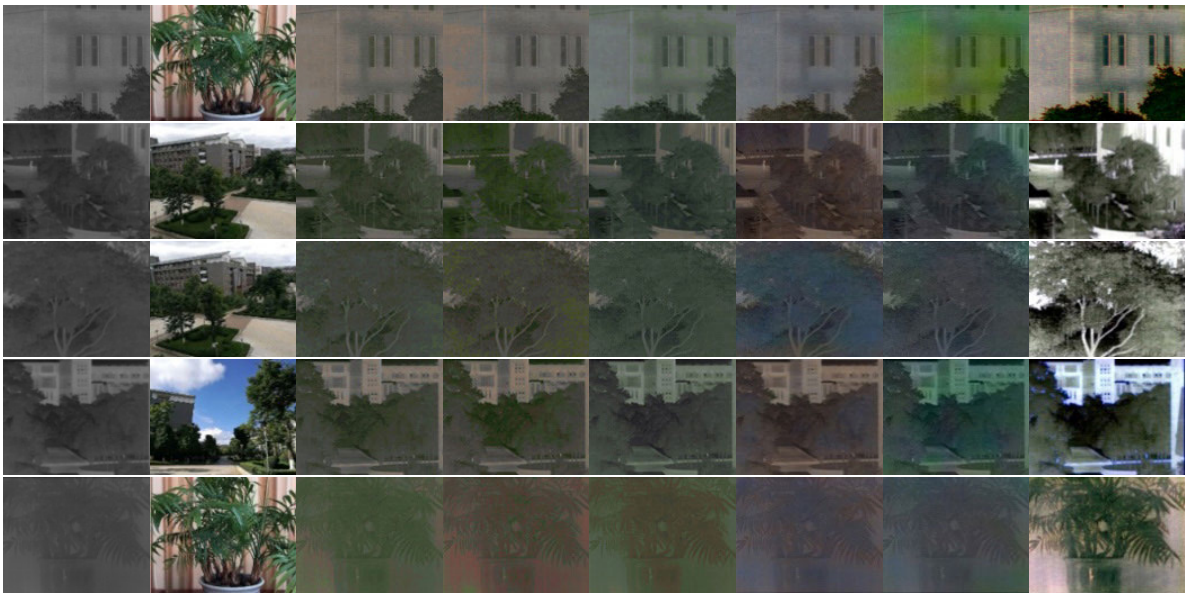

FIGURE 8. Colorization results:(a) Infrared image acquired by our hardware platform; (b) Reference source image; (c) Welsh method [14]; (d) Li method [15]; (e) Rajan Method [48]; (f) Iizuka method [26]; (g) Retrained Iizuka method; (h) Algorithm of this paper. From top to bottom are Image1, Image2, Image3, Image4, and Image5.

explanation [33]–[35]. This section present a physical explanation for the similarity between a haze image and an inverted infrared image in our new FC2F scheme.

A. ILLUMINATION MODEL OF AN INFRARED IMAGE

The literature [41] gives an infrared imaging illumination model based on Phong's model:

$$I = E_0(\lambda, T) + I_a k_a + k_d I_l \cos\theta + I_l k_s \cos^n T, \quad (16)$$

where I is the reflected intensity; $E_0(\lambda, T)$ is the source infrared radiation.T is the surface absolute temperature. k_a, k_d and k_s denote the ambient light reflection constant, the diffuse reflection constant and the specular reflection constant, respectively.

In the factors affecting the thermal image of an object, the surface temperature plays a major role [42]. We simplify the imaging model as:

$$I \approx E_0(\lambda, T). \quad (17)$$

The spectral radiant energy emission per unit time and per unit area from a blackbody at wavelength λ in the wavelength range $d\lambda$ is described by Planck's Law:

$$P_\lambda = \frac{2\pi hc^2}{\lambda^5} \frac{1}{e^{hc/(\lambda kT)} - 1} = \frac{C_1}{\lambda^5} \frac{1}{e^{C_2/(\lambda T)} - 1}, \quad (18)$$

where P_λ is the spectral radiant emittance of a blackbody at absolute temperature T. λ is the wavelength; C_1 is the first radiation constant, C_1=3.742 $\times$ $10^{-16} W \bullet m^2$; C_2 is the second radiation constant, C_2=1.4388 $\times$ $10^{-2} m \bullet K$.

At the same temperature, the general object's radiation ability is worse than the blackbody. It can be corrected by multiplying $X_0 (0 < X_0 < 1)$. Therefore when we simulate the infrared images of the object, the radiance of the object surface can be calculated using Planck's Law:

$$E_0(\lambda, T) \approx X_0 \int_{\lambda_1}^{\lambda_2} \frac{C_1}{\lambda^5} \frac{1}{e^{C_2/(\lambda T)} - 1} d\lambda. \quad (19)$$

Using the partial integral method, we can approximately evaluate this integral as below: when the wavelength and temperature are determined, the source infrared radiation E_0 can be calculated according to (19), which can be regarded as a constant.

The transmitted radiation through the medium with a distance R from a source radiation E_0 at wavelength λ is described by Bouguer-Lambert law [43]:

$$I_{infrared} = I \cdot e^{-\mu(\lambda)d} \approx E_0(\lambda) e^{-\mu(\lambda)d}, \quad (20)$$

where $\mu(\lambda)$ = extinction coefficient, d = pathlength. $\mu(\lambda)$ is composed of absorption and scattering, and is closely related to atmospheric conditions. **The radiation $I_{infrared}$ received by the infrared thermal imaging system obeys an exponential relationship.**

B. THE FORMATION MODEL OF A HAZE IMAGE

In a haze image, two fundamental phenomena which degrade the image visibility are attenuation and air light [44]. Mathematically, the attenuation is modelled as an exponential function given by (21):

$$Attenuation = J \cdot e^{-k(\lambda)d}, \quad (21)$$

where J is the original image when fog is not present in the atmosphere, k is the extinction coefficient and d is the distance of scene point from the camera, called **scene depth**.

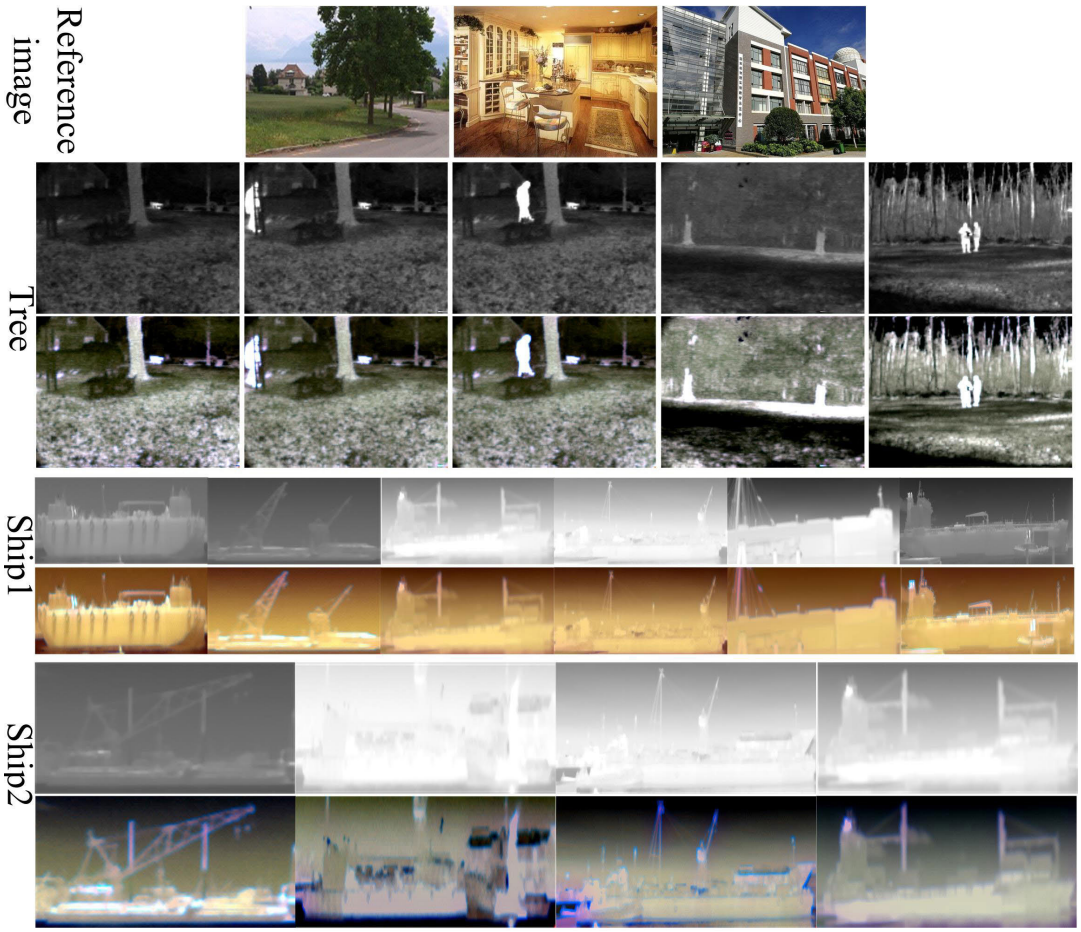

FIGURE 9. Colorization results by the proposed method: Top row: Left is the reference image of Tree group. Middle is the reference image of Ship1 group. Right is the reference image of Ship2 group.

FIGURE 10. The comparison results of different algorithms: Left is the original image. Middle is the result obtained by the minimum filter method. Right is the result obtained by the proposed method.

Air light is represented as a function of atmospheric light and scene depth shown in (22).

$$Airlight = A(1 - e^{-k(\lambda)d}), \tag{22}$$

where A represents the atmospheric light constant which is sometimes called the intensity of the sky. According to the Schechner *et al.* [45], Tarel and Hautiere [46], and Koschmieder [47] effect of fog on the image is represented as:

$$I_{fog}(x, y) = Attenuation + Airlight. \tag{23}$$

Now, the Koschmieder law can also be represented as follow:

$$I_{fog} = J \cdot e^{-k(\lambda)d} + A(1 - e^{-k(\lambda)d}). \tag{24}$$

FIGURE 11. Improvement of detail and natural presentation of colors: Left is the result obtained by Reinhard *et al.*'s algorithm; Right is the result obtained by Our algorithm.

Finally, by rearranging the above equations, we will get:

$$\begin{aligned} I_{fog} &= A - Ae^{-k(\lambda)d} + J \cdot e^{-k(\lambda)d} \\ \frac{I_{fog}}{A} &= 1 - e^{-k(\lambda)d} + \frac{J}{A}e^{-k(\lambda)d} \\ \frac{I_{fog}}{A} &= 1 - (1 - \frac{J}{A})e^{-k(\lambda)d}. \end{aligned} \tag{25}$$

Under certain conditions, the formation model of a haze image shown in (25) and the illumination model of an

FIGURE 12. Colorization results by the proposed method for near infrared images.

infrared image shown in (20) are complementary. When $A = 1$, $E_0 = (1 - \frac{J}{A})$ and $\mu(\lambda)d = k(\lambda)d$, it can be inferred:

$$I_{fog} = 1 - E_0(\lambda)e^{-\mu(\lambda)d} = 1 - I_{infrared}, \tag{26}$$

where $E_0(\lambda)$ and J are all independent of the distance. They can be regarded as constant.

The similarity is explained from the perspective of physical mechanism. n addition, we notice that the inverted infrared image looks very much similar to foggy images with a similar scene or style, as shown in Figure 5. Figure 5 provides some examples of infrared images, inverted infrared images and images acquired with haze. As mentioned in [36], the background of fog images present a white and misty visual effect, and its intensity is very high in all RGB channels. The intensity of the main objects, such as houses, vehicles, and people, etc., is usually at a low brightness in at least one channel. It is because of several facts, such as colors and shadows. However, in infrared images, the intensities of the background pixels are usually low, and the intensities of the main objects are rather high. Therefore, an inverted and infrared image has exactly the same properties to that the corresponding haze image. To better explain this phenomenon, we need RGB-IR image pairs acquired in hazy lighting conditions of the same set of pictures. However, there is not a public RGB–IR image pair database available yet. Instead, we have further made a set of new comparison on 30 haze images with a similar scene or style. Similar scenes could mean that there are buildings, person, tree, hands in both of fog and inverted infrared images. Similar style could be of both images showing a dimly similar style.

To test whether the inverted infrared image has the same property as the haze image or not, we compute the histogram of the intensities (the grayscale value) for the 30 inverted infrared images captured by our infrared camera. To better explain this phenomenon, we need RGB-IR image pairs acquired in hazy lighting conditions of the same set of pictures. However, the public RGB–IR image pair database with haze is not yet available. Instead, we add a set of new evaluation on the histogram of the minimum intensity of all color (RGB) channels for each pixel of 30 haze images that were randomly selected on Google. Figure 6 shows the histogram of the intensities for 30 haze images and 30 inverted infrared images. The two histograms exhibit great similarities. More than 80% of pixels in both the inverted and the haze cases have high intensities. In the histograms, the grayscale value ranging from 0 to 255 is divided into 5 equal parts. These equal parts are known as bins or class intervals. Every observation (or value) in the image is placed in an appropriate bin. The occurrence of intensity level occupying a bin is used to estimate the probability.

V. EXPERIMENTS, EVALUATION AND ANALYSIS

To evaluate the new FC2F scheme, we develop an experimental system in our laboratory, as shown in Figure 7, which

FIGURE 13. Colorization results by the proposed method for low-illumination images.

includes two-way videos. The hardware system includes JN-MINI5728 core board, JN-miniVB bottom board, FLIR core Tau2-336 uncooled thermal long wavelength IR detector, SONY ICX639AK CCD and the remote host computer. We use the pictures with a spatial resolution of 640 × 480 pixels and test the algorithm in the Matlab2019 environment on a Pentium host with a frequency of 2.20 GHz and 1 GB of memory. The proposed algorithm is subjectively and objectively evaluated. It is compared with Welsh *et al.*'s algorithm [14], Li *et al.*'s algorithm [15], Rajan's algorithm [48], Iizuka *et al.*'s algorithm [26] and retrained Iizuka *et al.*'s algorithm. Since the training data set used by the Iizuka *et al.*'s algorithm is human faces, the result of the processing is yellowish. The forest images are re-selected for training, which is called the retrained Iizuka method.

A. SUBJECTIVE EVALUATION

Figure 8 shows the results of different algorithms. The original infrared image often suffers from low contrast, poor spatial resolution and unclear details, as shown in Figure 8 (a). Our result image is more natural coloring and detailed, as shown in Figure 8 (h). The color of the reference image for the approximate scene is successfully conveyed to the infrared image. The infrared image with a very narrow grayscale range is expressed in the form of a more extensive dynamic range. It is significantly better than existing techniques, as shown in Figure 8 (c) (d) (e) (f) (g). Furthermore, the new FC2F scheme was performed on the Thermal World dataset [49], [50]. It produces excellent results, as shown in Figure 9.

B. OBJECTIVE EVALUATION

Since the human eye is not sensitive to chromaticity change, we convert the color image in RGB space into the YCbCr space, and then we evaluate the luminance component. The objective results of the algorithm are evaluated by five objective indicators: average gradient, entropy, edge intensity, contrast and clarity, as shown in Table 1. The data in Table 1 is for Image1, Image2, Image3, Image4, and Image5 in Figure 8. It can be seen from Table 1 that the five objective indicators of the result processed by our method are much advanced, and especially the contrast is significantly improved.

(1) Average gradient (AG): A larger AG means that the image has a higher contrast and clearer texture features. The definition is given as:

$$AG = \frac{1}{M \times N} \sum_{x=1}^{M} \sum_{y=1}^{N} \sqrt{\frac{[\Delta_x f(x,y)]^2 + [\Delta_y f(x,y)]^2}{2}}, \quad (27)$$

where $f(x, y)$ is the pixel value of the result image at the position (x, y). $\Delta_x f(x, y)$ and $\Delta_y f(x, y)$ represent the differential operators along the x and y directions of the resulting image.

They can be represented as follows:

$$\Delta_x f(x,y) = f(x,y) - f(x+1,y), \tag{28}$$
$$\Delta_y f(x,y) = f(x,y) - f(x,y+1). \tag{29}$$

(2) Entropy (EN) [51]: Entropy is used in information theory to measure how much information contained and we can define it as:

$$EN = -\sum_{i=0}^{L-1} p(i)\log_2 p(i), \tag{30}$$

where $p(i)$ is the gray frequency of a result image, and L is the gray level of the result image.

(3) Edge intensity (EI): The sobel edge detection operators are convolved with the result image f to calculate approximations of the derivatives–G_x for horizontal changes, and G_y for vertical:

$$G_x = \begin{bmatrix} 1 & 0 & -1 \\ 2 & 0 & -2 \\ 1 & 0 & -1 \end{bmatrix} * f, \tag{31}$$

$$G_y = \begin{bmatrix} 1 & 2 & 1 \\ 0 & 0 & 0 \\ -1 & -2 & -1 \end{bmatrix} * f. \tag{32}$$

EI is the average magnitude of the gradient of the edge points. The definition is given as:

$$EI = \frac{1}{M \times N} \sum_{i=1}^{M} \sum_{j=1}^{N} \sqrt{{G_x}^2 + {G_y}^2}. \tag{33}$$

(4) Contrast: The mean−square difference between the center pixel and the 8−neighboring pixel is adopted as contrast. The larger the contrast, the richer the detail. The definition is given as:

$$Contrast = \frac{1}{M \times N} \sum_{x=1}^{M} \sum_{y=1}^{N} Contrast_{Local}(x,y), \tag{34}$$

where $Contrast_{Local}(x,y)$ is the local contrast at the position (x,y). It can be represented as follows:

$$Contrast_{Local}(x,y) = \sum_{i=-1}^{1} \sum_{j=-1}^{1} [f(x+i,y+j) - f(x,y)]^2. \tag{35}$$

(5) Clarity: The sum of the product of adjacent pixels difference in the horizontal and vertical direction is used as core function to evaluate clarity. The definition is given as:

$$Clarity = \sum_{x=1}^{M} \sum_{y=1}^{N} I_p(x,y), \tag{36}$$

where $I_p(x,y)$ is the product of adjacent pixels difference. It can be represented as follows:

$$I_p(x,y) = [f(x,y) - f(x+1,y)][f(x,y) - f(x,y+1)]. \tag{37}$$

FIGURE 14. Different pair of source and target images that presents different style: The result's quality depends on the source images'style.Top row: target image; Middle row: result image; Bottom row: reference image.

FIGURE 15. Failure case: We say it fails when the result image haven't the source image's feel and look.Left is the target image. Middle is the source image. Right is the result image.

C. ANALYSIS AND DISCUSSION

In this section, we will use various techniques to establish related space and realize the fine colorization. In addition, some defects and extensions to low illumination and near-infrared images will be discussed simultaneously.

1) TECHNICAL ANALYSIS OF VARIOUS COLORIZATION

- Another R channel illumination map estimation

$$T_r(I) \leftarrow \min_{y \in \Omega(x)} (I(y)). \tag{38}$$

If we adopt (38) as the R channel instead of (3), the comparison result is shown in the Figure 10. The minimum filter brings the block effect. It is necessary to try to avoid hallo effect when constructing the relevant space.

- Another combination of coarse and fine colorization

$$T_{r,g,b}(I) \leftarrow I. \tag{39}$$

Equation (39) is taken as the coarse colorization method and Reinhard *et al.*'s algorithm [12] is considered as the fine colorization method. Equation (39) can build a coarse colorization image which has strong correlation between RGB channels. In addition, Reinhard *et al.*'s algorithm [12] can also manipulate the point set of the target image to match the point set of the source image. In a rough look, this is comparable to the strategy of this paper. But, our result is more natural presentation of colors and more detailed, as shown in Figure 11 and Table 2. It can be seen from Table 2 that the five objective indicators of the result processed by our method

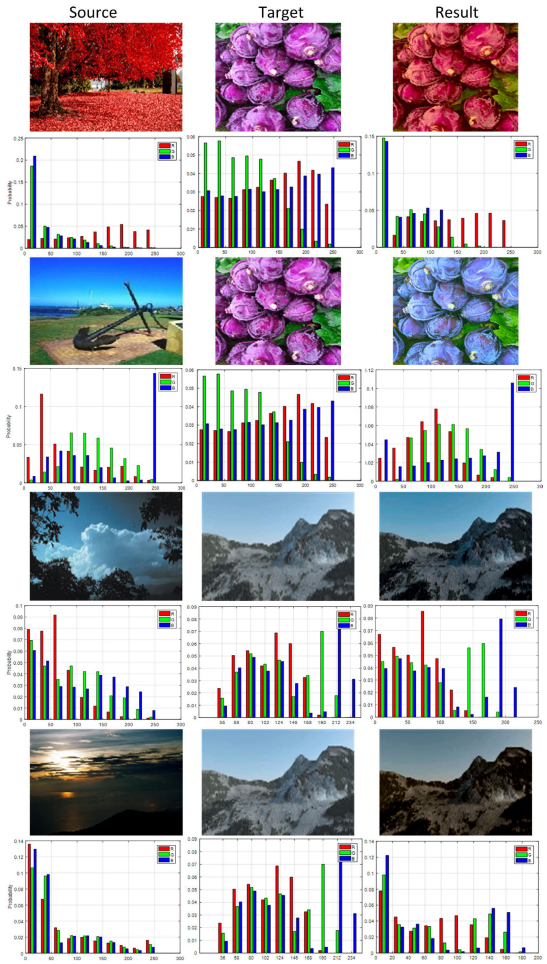

FIGURE 16. Comparison of color histograms: when color transfer has been done by the fine colorization method, the color histograms will have a similar distribution trend. And the choice of reference image directly affects the final result.

TABLE 1. Comparison of different algorithms in terms of five objective indicators.

Algorithm		Average gradient	Entropy	Edge intensity	Contrast	Clarity
Original image	Image1	2.32	5.81	23.08	65.33	2.75
	Image2	2.93	5.94	30.07	160.27	3.43
	Image3	2.34	5.04	24.47	65.02	2.99
	Image4	1.79	6.12	18.92	14.49	2.19
	Image5	1.82	4.74	17.57	41.98	2.07
Welsh[15]	Image1	2.49	5.87	24.83	58.67	3.09
	Image2	2.07	5.83	21.41	17.53	2.44
	Image3	2.3	4.96	23.3	21.54	3.12
	Image4	2.54	6.09	24.7	99.26	2.95
	Image5	1.36	4.69	13.92	7.27	1.67
Li[16]	Image1	1.7	5.8	18.01	10.1	2.06
	Image2	2.18	5.9	22.16	38.2	2.44
	Image3	1.78	4.96	18.7	10.41	2.18
	Image4	1.58	6.12	16.96	8.12	1.87
	Image5	1.19	4.69	12.36	4.48	1.45
Rajan[36]	Image1	1.68	5.79	17.88	9.83	2.06
	Image2	2.13	5.88	21.8	33.54	2.4
	Image3	2.12	4.99	21.31	35.36	2.45
	Image4	1.63	6.12	17.51	8.98	1.98
	Image5	1.23	4.71	12.75	4.74	1.48
Iizuka[22]	Image1	1.45	5.77	15.48	7.47	1.69
	Image2	1.61	5.87	17.28	8.19	1.84
	Image3	1.52	4.94	16.16	7.17	1.78
	Image4	2.04	6.17	20.23	59.32	2.07
	Image5	0.68	4.59	7.35	1.33	0.75
Retrained Iizuka	Image1	1.03	5.78	11.41	4.06	1.11
	Image2	1.46	5.93	16.14	9.73	1.53
	Image3	1.42	5.01	15.53	17.81	1.49
	Image4	1.17	6.15	12.92	4.84	1.23
	Image5	0.76	4.74	8.35	2.34	0.82
Our method	Image1	**4.07**	**6.89**	**42.57**	**131.6**	**5.28**
	Image2	**5.53**	**7.34**	**57.9**	**228.5**	**6.51**
	Image3	**8.62**	**7.35**	**88.9**	**334.7**	**11.09**
	Image4	**5.05**	**7.5**	**51.57**	**194.4**	**6.25**
	Image5	**6.66**	**7.26**	**66.36**	**185.7**	**9.61**

TABLE 2. Comparison of the two algorithms in terms of five objective indicators.

Algorithm	Average gradient	Entropy	Edge intensity	Contrast	Clarity
Reinhard	5.5	6.93	57.58	89.21	6.68
Our method	**6.66**	**7.26**	**66.36**	**185.7**	**9.61**

are greatly improved. One reason is that the guide filter plays a vital role in enhancing the details. The other reason is that Xiao *et al.*'s algorithm [13] increases the rotation operation.

2) NEW APPLICATION AND IMAGE DEPENDENCE

Near-infrared images and low-illumination images are also single-channel images, and the algorithm has achieved good results as well. The experimental results are shown in the Figure 12 and Figure 13. Not only natural coloring is made but also the detail enhancement is achieved.

Because we want to transfer one image's style to appear in another image, we may unfortunately choose inappropriate image pairs. The result's quality depends on the source images' style, as shown in Figure 14. sometimes the source image and the target image do bad things together, as shown in Figure 15. Some ideas have been suggested, such as a samples-based approach [12] or providing some parameters through a more flexible user interaction [13].

We show how the choice of reference image significantly affects the final result applying the fine colorization algorithm between visible light images in Figure 16. The resulting quality depends on the two images' similarity in color composition. Moreover, the fine colorization algorithm does not require choosing the same color style and imaging size between input and reference images. It was global approach reshaping the input image color histogram to match the histogram of the reference image. As shown in Figure 16, when colorization has been done by the fine colorization method in this paper, the color histograms of the result image will have a similar distribution trend with the reference image. However, if the reference image is too different in color composition to the input, global methods such as the one discussed, cannot guarantee that the color mapping will be successful.

Selecting a source image needs to consider many factors, such as the similar content structure information of input images, the similar textural information surrounding

each pixel, the similar scene, the similar style and the characteristics of human color perception, etc. In this way, colors may be transferred only between highly similar regions, such as the sea or the clouds of the source and target images. However, if the target image contains complex scenes, it is difficult to find a satisfactory source image that can offer adequate color for all different input regions. To our best knowledge, subjective judgment is the main widely adopted method to evaluate the quality of the transferred image in previous color transfer algorithms. It is meaningful to find an effective objective metrics. Then the objective metrics can be applicable for selecting a reference image for a colored target image and we can finally built an image database after experimenting with the proposed metrics in the future.

VI. CONCLUSION

In this paper, we presented a new colorization scheme for infrared image enhancement and colorization. The new scheme has two stages: coarse colorization and fine colorization. An explainable theoretical study was provided to support the new scheme. We conducted a number of well designed experiments on the well-known image datasets to evaluate the performance of the new scheme. The results demonstrated that the new scheme outperformed other state-of-the-art methods in terms of both subjective and objective measures. The new scheme is applicable to the colorization of low illumination images and near-infrared images.

REFERENCES

[1] X. Gong, Q. Yao, M. Wang, and Y. Lin, "A deep learning approach for oriented electrical equipment detection in thermal images," *IEEE Access*, vol. 6, pp. 41590–41597, 2018.
[2] B. L. Jian, C. Chen, M. W. Huang, and H. Yau, "Emotion-specific facial activation maps based on infrared thermal image sequences," *IEEE Access*, vol. 7, pp. 48046–48052, 2019.
[3] Q. Zhang, Y. Zhou, S. Song, G. Liang, and H. Ni, "Heart rate extraction based on near-infrared camera: Towards driver state monitoring," *IEEE Access*, vol. 6, pp. 33076–33087, 2018.
[4] M. He, J. Liao, D. Chen, L. Yuan, and P. V. Sander, "Progressive color transfer with dense semantic correspondences," *ACM Trans. Graph.*, vol. 38, no. 2, pp. 1–18, Apr. 2019.
[5] F. Fang, T. Wang, T. Zeng, and G. Zhang, "A superpixel-based variational model for image colorization," *IEEE Trans. Vis. Comput. Graphics*, early access, Mar. 29, 2019, doi: 10.1109/TVCG.2019.2908363.
[6] H. Liu, Z. Fu, J. Han, L. Shao, and H. Liu, "Single satellite imagery simultaneous super-resolution and colorization using multi-task deep neural networks," *J. Vis. Commun. Image Represent.*, vol. 53, pp. 20–30, May 2018.
[7] R. Zhang, P. Isola, and A. A. Efros, "Colorful image colorization," in *Proc. Eur. Conf. Comput. Vis.* Amsterdam, The Netherlands: Springer, 2016, pp. 649–666.
[8] B.-W. Chen, X. He, W. Ji, S. Rho, and S.-Y. Kung, "Large-scale image colorization based on divide-and-conquer support vector machines," *J. Supercomput.*, vol. 72, no. 8, pp. 2942–2961, Aug. 2016.
[9] S. Liu and X. Zhang, "Automatic grayscale image colorization using histogram regression," *Pattern Recognit. Lett.*, vol. 33, no. 13, pp. 1673–1681, Oct. 2012.
[10] Q. Song, F. Xu, and Y.-Q. Jin, "Radar image colorization: Converting single-polarization to fully polarimetric using deep neural networks," *IEEE Access*, vol. 6, pp. 1647–1661, 2018.
[11] W. Ye, H. Chen, Z. Zhang, Y. Liu, S. Weng, and C.-C. Chang, "Hybrid scheme of image's regional colorization using mask R-CNN and Poisson editing," *IEEE Access*, vol. 7, pp. 115901–115913, 2019.
[12] E. Reinhard, M. Adhikhmin, B. Gooch, and P. Shirley, "Color transfer between images," *IEEE Comput. Graph. Appl.*, vol. 21, no. 4, pp. 34–41, Jul./Aug. 2001.
[13] X. Xiao and L. Ma, "Color transfer in correlated color space," in *Proc. ACM Int. Conf. Virtual Reality Continuum Appl. (VRCIA)*, 2006, pp. 305–309.
[14] T. Welsh, M. Ashikhmin, and K. Mueller, "Transferring color to greyscale images," in *Proc. 29th Annu. Conf. Comput. Graph. Interact. Techn. (SIGGRAPH)*, 2002, pp. 277–280.
[15] C. Li, J. Shi, L. Wei, and L. Xu, "Color fusion of night vision image based on wavelet transformation and color transfer," *Laser Infr.*, vol. 46, no. 5, pp. 607–611, 2016.
[16] F. Pitie, A. C. Kokaram, and R. Dahyot, "N-dimensional probability density function transfer and its application to color transfer," in *Proc. 10th IEEE Int. Conf. Comput. Vis. (ICCV)*, vol. 1, Oct. 2005, pp. 1434–1439.
[17] D. Freedman and P. Kisilev, "Object-to-object color transfer: Optimal flows and SMSP transformations," in *Proc. IEEE Comput. Soc. Conf. Comput. Vis. Pattern Recognit.*, Jun. 2010, pp. 287–294.
[18] Y. LeCun, Y. Bengio, and G. Hinton, "Deep learning," *Nature*, vol. 521, pp. 436–444, May 2015.
[19] S. Wen, W. Liu, Y. Yang, T. Huang, and Z. Zeng, "Generating realistic videos from keyframes with concatenated GANs," *IEEE Trans. Circuits Syst. Video Technol.*, vol. 29, no. 8, pp. 2337–2348, Aug. 2019.
[20] I. Goodfellow, Y. Bengio, and A. Courville, *Deep Learning*. Cambridge, MA, USA: MIT Press, 2016.
[21] N. Sun, J. Zhang, P. Rimba, S. Gao, L. Y. Zhang, and Y. Xiang, "Data-driven cybersecurity incident prediction: A survey," *IEEE Commun. Surveys Tuts.*, vol. 21, no. 2, pp. 1744–1772, 2nd Quart., 2019.
[22] L. Liu, O. De Vel, Q.-L. Han, J. Zhang, and Y. Xiang, "Detecting and preventing cyber insider threats: A survey," *IEEE Commun. Surveys Tuts.*, vol. 20, no. 2, pp. 1397–1417, 2nd Quart., 2018.
[23] Z. Cheng, Q. Yang, and B. Sheng, "Deep colorization," in *Proc. IEEE Int. Conf. Comput. Vis. (ICCV)*, Dec. 2015, pp. 415–423.
[24] G. Patterson and J. Hays, "SUN attribute database: Discovering, annotating, and recognizing scene attributes," in *Proc. IEEE Conf. Comput. Vis. Pattern Recognit.*, Jun. 2012, pp. 2751–2758.
[25] E. Tola, V. Lepetit, and P. Fua, "A fast local descriptor for dense matching," in *Proc. IEEE Conf. Comput. Vis. Pattern Recognit.*, Jun. 2008, pp. 1–8.
[26] S. Iizuka, E. Simo-Serra, and H. Ishikawa, "Let there be color!: Joint end-to-end learning of global and local image priors for automatic image colorization with simultaneous classification," *ACM Trans. Graph.*, vol. 35, no. 4, pp. 1–11, 2016.
[27] T. Sun, C. Jung, Q. Fu, and Q. Han, "NIR to RGB domain translation using asymmetric cycle generative adversarial networks," *IEEE Access*, vol. 7, pp. 112459–112469, 2019.
[28] M. Dong, S. Wen, Z. Zeng, Z. Yan, and T. Huang, "Sparse fully convolutional network for face labeling," *Neurocomputing*, vol. 331, pp. 465–472, Feb. 2019.
[29] A. Green, "Leveling airborne gamma-radiation data using between-channel correlation information," *Geophysics*, vol. 52, no. 11, pp. 1557–1562, 1987.
[30] J. A. Russer and P. Russer, "Modeling of noisy EM field propagation using correlation information," *IEEE Trans. Microw. Theory Techn.*, vol. 63, no. 1, pp. 76–89, Jan. 2015.
[31] J. Zhang, Y. Xiang, Y. Wang, W. Zhou, Y. Xiang, and Y. Guan, "Network traffic classification using correlation information," *IEEE Trans. Parallel Distrib. Syst.*, vol. 24, no. 1, pp. 104–117, Jan. 2013.
[32] H. Palus, "Representations of colour images in different colour spaces," in *The Colour Image Processing Handbook*. Boston, MA, USA: Springer, 1998, pp. 67–90.
[33] L. Zheng, H. Shi, and M. Gu, "Infrared traffic image enhancement algorithm based on dark channel prior and gamma correction," *Mod. Phys. Lett. B*, vol. 31, nos. 19–21, Jul. 2017, Art. no. 1740044.
[34] X. Jiang, H. Yao, S. Zhang, X. Lu, and W. Zeng, "Night video enhancement using improved dark channel prior," in *Proc. IEEE Int. Conf. Image Process.*, Sep. 2013, pp. 553–557.
[35] X. Dong, G. Wang, Y. Pang, W. Li, J. Wen, W. Meng, and Y. Lu, "Fast efficient algorithm for enhancement of low lighting video," in *Proc. IEEE Int. Conf. Multimedia Expo*, Jul. 2011, pp. 1–6.
[36] K. He, J. Sun, and X. Tang, "Single image haze removal using dark channel prior," *IEEE Trans. Pattern Anal. Mach. Intell.*, vol. 33, no. 12, pp. 2341–2353, Dec. 2011.

[37] C. Liu, W. T. Freeman, R. Szeliski, and S. Bing Kang, "Noise estimation from a single image," in *Proc. IEEE Comput. Soc. Conf. Comput. Vis. Pattern Recognit.*, vol. 1, Jun. 2006, pp. 901–908.
[38] R. Fattal, M. Agrawala, and S. Rusinkiewicz, "Multiscale shape and detail enhancement from multi-light image collections," *ACM Trans. Graph.*, vol. 26, no. 3, p. 51, Jul. 2007.
[39] H. Winnemöller, S. C. Olsen, and B. Gooch, "Real-time video abstraction," *ACM Trans. Graph.*, vol. 25, no. 3, pp. 1221–1226, Jul. 2006.
[40] K. He, J. Sun, and X. Tang, "Guided image filtering," in *Proc. Eur. Conf. Comput. Vis.* Berlin, Germany: Springer, 2010, pp. 1–14.
[41] Z.-Y. Wang, Z.-Y. Jiang, H.-J. Bao, and Q.-S. Peng, "A quantity optics based illumination model for infrared image synthesis," *Chin. J. Comput.-Chin. Ed.*, vol. 25, no. 9, pp. 897–903, 2002.
[42] W. Yu, Q. Peng, H. Tu, and Z. Wang, "An infrared image synthesis model based on infrared physics and heat transfer," *Int. J. Infr. Millim. Waves*, vol. 19, no. 12, pp. 1661–1669, 1998.
[43] R. V. Maikala, "Modified Beer's Law–historical perspectives and relevance in near-infrared monitoring of optical properties of human tissue," *Int. J. Ind. Ergonom.*, vol. 40, no. 2, pp. 125–134, 2010.
[44] E. J. McCartney and F. F. Hall, "Optics of the atmosphere: Scattering by molecules and particles," *Phys. Today*, vol. 30, p. 76, Jan. 1977.
[45] Y. Y. Schechner, S. G. Narasimhan, and S. K. Nayar, "Instant dehazing of images using polarization," in *Proc. IEEE Comput. Soc. Conf. Comput. Vis. Pattern Recognit. (CVPR)*, vol. 1, Dec. 2001, pp. 1–8.
[46] J.-P. Tarel and N. Hautiere, "Fast visibility restoration from a single color or gray level image," in *Proc. IEEE 12th Int. Conf. Comput. Vis.*, Sep. 2009, pp. 2201–2208.
[47] H. Koschmieder, "Theorie der horizontalen Sichtweite," *Beitr. Phys. Freien Atmosph.*, pp. 33–53, 1924.
[48] J. Rajan. (2020). *Gray Image to Color Image Conversion*. MATLAB Central File Exchange. Accessed: Jun. 15, 2020. [Online]. Available: https://www.mathworks.com/matlabcentral/fileexchange/8214-gray-image-to-color-image-conversion
[49] R. Miezianko and D. Pokrajac, "People detection in low resolution infrared videos," in *Proc. IEEE Comput. Soc. Conf. Comput. Vis. Pattern Recognit. Workshops*, Jun. 2008, pp. 1–6.
[50] M. M. Zhang, J. Choi, K. Daniilidis, M. T. Wolf, and C. Kanan, "VAIS: A dataset for recognizing maritime imagery in the visible and infrared spectrums," in *Proc. IEEE Conf. Comput. Vis. Pattern Recognit. Workshops (CVPRW)*, Jun. 2015, pp. 10–16.
[51] K. Zhang, Y. Huang, X. Yuan, H. Ma, and C. Zhao, "Infrared and visible image fusion based on intuitionistic fuzzy sets," *Infr. Phys. Technol.*, vol. 105, Mar. 2020, Art. no. 103124.

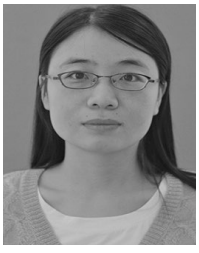

FEIYAN CHENG received the M.S. degree in circuits and systems from Lanzhou University, in 2010. She is a Teacher with the School of Information Science and Technology, Yunnan Normal University, China. Her research interests include color science and engineering, the characteristics of the human visual systems and its applications for color imaging, and digital image processing.

JUNSHENG SHI (Member, IEEE) received the M.S. degree in applied physics from the Hebei University of Technology, in 1994, and the Ph.D. degree in optical engineering from the Beijing Institute of Technology, in 2005. He is a Professor with the School of Physics and Electronics Information, Yunnan Normal University, China. His research interests include color science and engineering, the characteristics of the human visual systems and its applications for color imaging, and digital image processing.

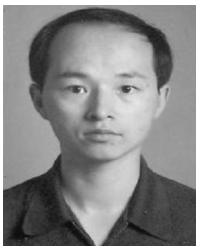

LIJUN YUN received the Ph.D. degree from the Hebei University of Technology, China. He is a Professor with the School of Information, Yunnan Normal University, China. His research interests include embedded development and photoelectric imaging.

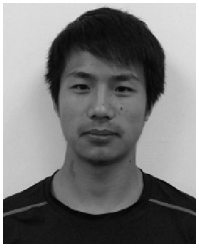

XUEBING CAO was born in Qujing, Yunnan, China, in 1998. He received the bachelor's degree in electronic information science and technology from Yunnan Normal University, in 2020. His current interests are in the areas of color science and digital image processing.

JUN ZHANG is a Professor with the School of Physics and Electronic Information, Yunnan Normal University, China. He has published over 100 research articles in refereed international journals and conferences such as the IEEE/ACM TRANSACTIONS ON NETWORKING, the IEEE TRANSACTIONS ON IMAGE PROCESSING, the IEEE TRANSACTIONSON PARALLEL AND DISTRIBUTED SYSTEMS, and the IEEE TRANSACTIONS ON INFORMATION FORENSICS AND SECURITY. His research interests include applied machine learning and data science. He has served as the chair of more than 20 international conferences.